International Journal of Nanomedicine Dovepress

Open Access Full Text Article ORIGINAL RESEARCH

Enhanced Bacterial and Biofilm Adhesion Resistance of ALD Nano-TiO_2 Coatings Compared to AO Coatings on Titanium Abutments

Yu Pan[1,*], Lili Cao[2,*], Libing Chen[1,*], Linjuan Gao[2], Xia Wei[1], Honglei Lin[1], Lei Jiang[1], Yinghui Wang[1,2], Hui Cheng[1,2]

[1]Department of Prosthodontics, Institute of Stomatology & Research Center of Dental Esthetics and Biomechanics, School and Hospital of Stomatology, Fujian Medical University, Fuzhou, Fujian, People's Republic of China; [2]Department of Prosthodontics, Fujian Key Laboratory of Oral Diseases & Fujian Provincial Engineering Research Center of Oral Biomaterial & Stomatological Key Laboratory of Fujian College and University, School and Hospital of Stomatology, Fujian Medical University, Fuzhou, Fujian, People's Republic of China

*These authors contributed equally to this work

Correspondence: Yinghui Wang; Hui Cheng, School and Hospital of Stomatology, Fujian Medical University, Fuzhou, Fujian, People's Republic of China, Email wyh9519@fjmu.edu.cn; ch.fj@fjmu.edu.cn

Purpose: The study was intended to compare the surface properties and the bacterial and biofilm adhesion resistance of two potential antibacterial nanometer titanium dioxide (nano-TiO_2) coatings on dental titanium (Ti) abutments prepared by atomic layer deposition (ALD) and the anodic oxidation (AO) techniques.

Methods: Nano-TiO_2 coatings were developed using ALD and AO techniques and applied to Ti surfaces. The surface properties and the bacterial and biofilm adhesion resistance of these coatings were evaluated against commonly used Ti and Zirconia (ZrO_2) surfaces. The chemical compositions, crystalline forms, surface topography, roughness and hydrophilicity were characterized. The antibacterial performance was assessed by the scanning electron microscope (SEM), the Colony-forming unit (CFU) assay and the 3-(4, 5-dimethylthiazolyl-2)-2, 5-diphenyltetrazolium bromide (MTT) assay using in vitro models of *Staphylococcus aureus* (*S. aureus*), *Streptococcus mutans* (*S. mutans*), and *Porphyromonas gingivalis* (*P. gingivalis*) in both single- and mixed-species bacterial compositions.

Results: ALD-prepared nano-TiO_2 coatings resulted in a dense, smooth, and less hydrophilic surface with an anatase phase, significantly reducing the adhesion of the three bacteria by over 50%, comparable to ZrO_2. In contrast, AO-prepared coatings led to a less hydrophilic surface, characterized by various nano-sized pores within the oxide film. This alteration, however, had no impact on the adhesion of the three bacteria. The adhesion patterns for mixed-species bacteria were generally consistent with single-species results.

Conclusion: ALD-prepared nano-TiO_2 coatings on Ti abutments demonstrated promising antibacterial properties comparable to ZrO_2 surfaces, suggesting potential in preventing peri-implantitis. However, the bacterial and biofilm adhesion resistance of AO-produced nano-TiO_2 coatings was limited.

Keywords: atomic layer deposition, anodic oxidation, titanium dioxide, dental abutment, surface properties, antibacterial effect

Introduction

Dental implant restorations have emerged as the preferred therapeutic modality for rehabilitating missing teeth, wherein the dental abutment stands as a pivotal component crucial to the soft tissue sealing.[1] Unfortunately, unlike the strong soft tissue sealing surrounding natural teeth, dental abutments exhibit significantly lower functional sealing performance. This discrepancy arises due to the fiber orientation being parallel to the abutment surface and the limited blood supply,

Received: 12 June 2024
Accepted: 18 October 2024
Published: 1 November 2024

Graphical Abstract

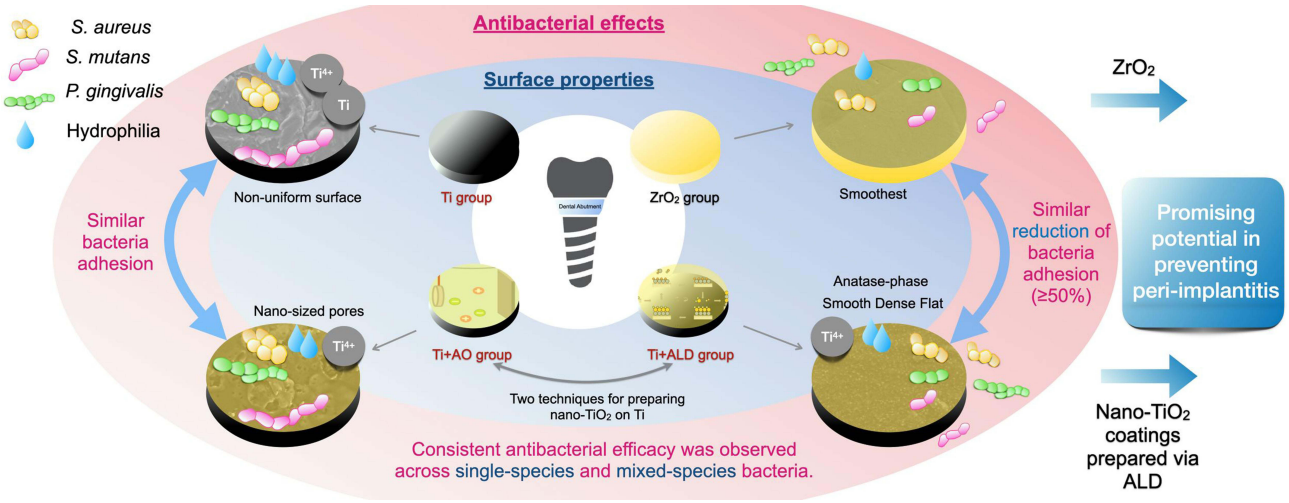

predominantly stemming from thin connective tissue.[2] Consequently, these conditions create a conducive environment for bacterial invasion and colonization on the surfaces of dental abutments. As biofilms migrate further, a cascade of tissue inflammation around the dental abutment is triggered.[3] This process can result in localized mucositis and, ultimately, advance to peri-implantitis. In contemporary clinical practice, commonly utilized implant abutment materials comprise titanium (Ti) and zirconia (ZrO_2). In a meta-analysis encompassing 19 clinical randomized controlled studies over an average observation period of 36 months, Sanz-Martin et al[4] observed a notable increase in mucosal inflammation reactions associated with Ti abutments compared to the ZrO_2 ones. The reasons for this discrepancy lie in the challenges posed by bacterial plaque adhesion on ZrO_2 surfaces.[5] This underscores the direct link between bacterial adhesion on implant abutment surfaces and the choice of materials. However, compared to Ti, the relatively low mechanical strength limits the widespread clinical application of ZrO_2. Thus, to mitigate the formation of biofilms and plaque accumulation, facilitating antibacterial ability on dental Ti abutments could prove beneficial. Given this context, nanometer titanium dioxide (nano-TiO_2) coatings exhibit broad-spectrum effectiveness against diverse microorganisms, encompassing Gram-positive and Gram-negative bacteria, among other types of microbes. Recent investigations have highlighted the ability of nano-TiO_2 coatings on dental implant materials to elicit an antibacterial effect on common bacteria,[6–9] usually with a rough surface.[9] It's worth noting that, surface treatments such as sandblasting and acid etching are commonly employed in the manufacturing of dental titanium implants to enhance surface roughness, facilitating osteoblast adhesion and proliferation, thereby improving osseointegration.[10] However, these treatments also increase bacterial adhesion.[11] In contrast, dental Ti abutments require a relatively smooth surface to promote the adhesion of surrounding soft tissue.[12] Consequently, machining and polishing are the preferred treatment for the emergence profile of dental Ti abutments at the manufacture, although it still offers limited antibacterial properties.[4]

There are two methods for preparing nano-TiO_2 coatings on dental Ti abutment materials. One is the anodic oxidation (AO) technology, a conventional and widespread coating preparation method, which has found extensive use in creating nano-TiO_2 coatings on surfaces of Ti-based materials like abutments (eg, Dentsply Astra Tech).[13] This process involves utilizing a metal as the anode in conjunction with an electrolyte such as sulfuric acid or phosphoric acid. When an external electric current is applied, oxidation reactions take place on the metal surface, resulting in the formation of an oxide layer. Moreover, this process can alter the surface characteristics and properties of the metal, encompassing factors such as surface color, biocompatibility, and corrosion resistance.[14] Studies indicated that nano-TiO_2 coatings produced through AO can enhance the hydrophilicity of Ti abutment surfaces[15] and facilitate the formation of anatase crystal structure TiO_2, consequently reducing early bacterial colonization on these surfaces.[16] However, findings from Hall

et al,[17] in a randomized controlled clinical study, revealed that compared to untreated Ti abutments, AO-modified Ti abutment surfaces did not significantly diminish bacterial biofilm formation. Nonetheless, they did note an enhancement in soft tissue integration on the material's surface. Consequently, the debate surrounding the antibacterial efficacy of AO-modified Ti abutments persists.

Another technology for the preparation of nano-TiO_2 coatings on dental Ti abutment materials is atomic layer deposition (ALD) technology, which has been described by our previous study.[18] It involves sequentially depositing materials in the form of atomic layers onto the surface of a substrate using alternating pulses of gas-phase precursors. This method can create uniform nano-scale coatings with controllable thickness and strong adhesion on micro or complex structures at relatively low temperatures,[19] showcasing its technological superiority compared to the AO technology. Studies highlighted ALD's capability in enhancing surface biocompatibility and curbing bacterial adhesion by modifying surface chemistry and nano structural morphology. This allows for precise control over surface nanostructure and surface energy.[9,18,20] Based on these advantages, nano-TiO_2 coatings synthesized via ALD exhibit promising antibacterial effectiveness across various applications, including orthopedic implants[9] and denture base materials.[21] Our previous study[18] also has indicated the ALD-TiO_2 coating with the thickness of 100 nm not only reduced bacterial adhesion but also exhibited favorable biocompatibility, corrosion resistance, and a warm yellow hue, enhancing the aesthetics of dental abutments. Thus, using ALD to create nano-TiO_2 coatings on dental Ti abutment surfaces holds significant clinical potential for imparting excellent antibacterial properties. However, whether the antibacterial effect of nano-TiO_2 coatings prepared by ALD is better than those produced by AO remains unknown.

The interface between the abutment and soft tissue, serving as the primary barrier against bacterial intrusion, is influenced not only by material surface properties but also by the diversity of bacteria involved.[22] Both Gram-positive and Gram-negative bacteria adhere and form biofilms through a multi-step process involving initial adhesion, irreversible attachment, maturation, and dispersion.[23,24] Initial bacterial attachment varies based on surface properties, while irreversible attachment is mediated by specific bacterial surface components.[24] The irreversible attachment is facilitated by surface structures like MSCRAMMs in Gram-positive bacteria and pili in Gram-negative bacteria, while extracellular polymeric substances (EPS) form a protective matrix.[25] Gram-negative bacteria rely on lipopolysaccharides (LPS), and Gram-positive bacteria on teichoic acids (TA), both of which provide surface charges that influence adhesion and biofilm formation. Quorum sensing (QS) regulates biofilm growth and dispersal, with Gram-positive bacteria using autoinducing peptides (AIP) and Gram-negative bacteria employing acyl-homoserine lactones (AHL).[24] Furthermore, Gram-positive bacteria boast thicker peptidoglycan layers, granting them higher resistance to reactive oxygen species (ROS), while the lipid layers and lipopolysaccharides of Gram-negative bacteria are more susceptible to disruption via photocatalytic means.[26]

Additionally, the oral microbial community exhibits considerable diversity and complexity, engaging in interactions such as symbiosis, competition, and antagonism.[27] Regarding the mixed-species models, Dorkhan et al[16] found bacterial adhesion to anodized Ti surfaces involving early colonizers (*oral streptococci, viridans streptococci, Aggregatibacter actinomycetemcomitans*, and *Streptococcus sanguinis*) revealed reduced adhesion for mixed-species and single-species after 2 hours compared to commercially pure Ti. However, the reduction in mixed-species adhesion did not yield statistically significant differences. Similarly, Mouratidou et al[28] established single-species bacterial biofilms (*Actinomyces naeslundii, Fusobacterium nucleatum*, and *Streptococcus gordonii*) alongside mixed-species biofilms to explore antibiotic sensitivity. Their findings highlighted that mixed-species biofilms displayed reduced antibiotic sensitivity compared to single-species biofilms. Consequently, developing models involving both single-species and mixed-species biofilms becomes indispensable in studying the antibacterial effectiveness of abutment materials, providing a more accurate comprehension of the intricate interplay between oral microbiota and diverse materials.

Therefore, the present study aims to compare the surface properties of nano-TiO_2 coatings applied to dental Ti abutments, fabricated by ALD and AO techniques. This evaluation will be assessed in comparison with ZrO_2 and Ti surfaces. To further investigate the bacterial and biofilm adhesion resistance of these four surfaces, in vitro bacterial models were employed, encompassing single-species and mixed-species compositions of three peri-implantitis-associated bacteria, such as the Gram-negative obligate anaerobe *P. gingivalis*, and Gram-positive obligate anaerobe *S. mutans*, and *S. aureus*. The results of this investigation would establish the foundational knowledge regarding the performance of these materials as dental abutment materials in the oral cavity and offer recommendations for dental abutment materials

to help prevent peri-implantitis. The hypotheses under investigation are as follows: (1) Distinct differences exist in surface properties among the four surfaces. (2) Discrepancies are observed in the bacterial adhesion of *S. mutans, S. aureus*, and *P. gingivalis* on these four surfaces. (3) Variances emerge in the adhesion of mixed-species bacteria to the four materials compared to the adhesion observed with single-species compositions.

Materials and Methods

This study did not involve humans or animals and did not require ethics approval.

Preparation of Materials

In this study, two dental materials, Ti (Ti6Al4V, Nissin, China) and ZrO_2, (Aidite, China) were utilized. Test samples were designed as disk-shaped specimens (10.0 mm in diameter, 2.0 mm in thickness) and they were fabricated by the computer-aided design and computer-aided manufacturing (CAD-CAM) mill. All specimens were wet-polished with silicon carbide sandpapers to grade #7000. Subsequently, they were sequentially cleaned and dried with acetone, ethanol, and deionized water using ultrasonication. *That were Ti group and ZrO_2 group.*

And then, two methods were used to prepare the nano-TiO_2 coatings on Ti surface. The first method, ALD technology, was described as follows: the samples were placed in the ALD (TALD-06G, Jiaxingkeming, China), operating in thermal mode. The nano-TiO_2 coatings were then applied to the Ti substrates using Titanium tetrakis dimethylamide (TDMAT) and H_2O as precursors, along with argon (99.999%) as the purge gas. Each ALD cycle in this study consisted of a 0.1-second TDMAT, a 25-second argon purge, a 0.02-second H_2O purge, and another 25-second argon purge. The nano-TiO_2 coatings were grown at a temperature of 260°C, with a total of approximately 1625 cycles prepared. And then the nano-TiO_2 coatings with the thickness of 100 nm were produced. *That were Ti+ALD group*. Following the treatments, the samples were rinsed with deionized water and the hot air dried.[8,15]

The second method employed in this study involved the utilization of AO technology. Electrochemical staining was conducted on Ti samples using a 1M phosphoric acid electrolytic solution within a temperature-regulated enclosure (DH1719A-5 model, Dahua, China). The Ti was affixed to the anode, while a 20.0 mm × 30.0 mm stainless steel plate served as the cathode, positioned at a distance of 2 cm from the anode. A constant voltage of 60 V was applied through a direct current stabilizing power supply (DH1719A-5 model) for a duration of 60 seconds to facilitate AO. The specific reaction process is outlined as follows:[24] Upon application of an appropriate oxidation voltage, the anode sheds electrons, generating Ti^{4+} ions according to formula (1). Simultaneously, O^{2-} ions and OH^- ions manifest at the cathode as indicated in formula (2). These resulting ions migrate via the electric field and electrolyte transport. The interaction of Ti^{4+} ions with O^{2-} ions leads to the formation of TiO_2 at the titanium/electrolyte interface, outlined in formula (3). *That were Ti +AO group*. Following the treatments, the samples were rinsed with deionized water and hot air dried.[8,15]

$$Ti - 4e^- \rightarrow Ti^{4+} \quad (1)$$

$$2OH^- + 2e^- \rightarrow 2O^{2-} + H_2 \uparrow \quad (2)$$

$$Ti^{4+} + 2O^{2-} \rightarrow TiO_2 \quad (3)$$

Subsequently, all the samples from four groups were stored after sterilization with ethylene oxide gas.

Surface Properties

Chemical Analysis

The chemical compositions of the randomly selected samples from Ti, Ti+AO and Ti+ALD groups were determined by the X-ray photoelectron spectroscopy (XPS) system (Thermo Scientific K-Alpha+, Thermo Fisher, USA).

Crystalline Forms Analysis

The crystalline forms of the randomly selected samples from Ti, Ti+AO, and Ti+ALD groups were performed using X-ray diffraction (XRD) (Miniflex 600, Rigaku, Japan) equipped with Cu Kα radiation.

Surface Topography and Roughness Analysis

The randomly selected samples from four groups were subjected to surface topography and roughness analysis. The scanning electron microscope (SEM) device (Sigma 300, Zeiss, Germany) was used for surface topography evaluation. The non-conductive ZrO_2 samples were gold-sputtered, and then the samples were placed in the SEM device at magnifications of × 5.00 K, and × 20.00 K. Atomic Force Microscope (AFM) (Dimension Icon, Bruker, USA) was used for roughness analysis.

Hydrophilicity

The hydrophilicity of the samples from each group (n = 6) was assessed through water contact angle (WCA) measurements. Using an optical contact angle meter (SDC-100, Shengding, China), a 4 μL drop of distilled water was placed on the specimen's surface. Final contact angle values were determined by averaging three measurements taken at different parts of the surfaces.

Antibacterial Assays

Single-Species Biofilm Formation

S. aureus (ATCC 25,923), *S. mutans* (ATCC 25,175), and *P. gingivalis* (ATCC 33,277) were cultured as described in the previous study.[18]

Mixed-Species Biofilm Formation

Single-species biofilm formation was conducted following the protocol as described in a previous study.[18] The concentrations of *S. aureus, S. mutans*, and *P. gingivalis* were subsequently adjusted to 1×10^8 CFU/mL, with *S. mutans* and *S. aureus* further diluted to 1×10^3 CFU/mL. These three bacterial suspensions were combined in equal proportions. Subsequently, the samples were placed into 15 mL centrifuge tubes (n = 6), and 200 μL of the aforementioned suspensions were added to each tube, supplemented with 5 mL of brain heart infusion (BHI) culture medium, constituting the mixed microbial solution for this study. These samples were then transferred to 24-well plates (n = 6), where 100 μL of the same suspensions were added to each well, along with 1 mL of bacterial culture medium. The plates were subsequently incubated at 37°C for 24 hours.

Colony-forming Unit (CFU) Counts

After a 24-hour incubation period, the samples (n = 6) with single-species or mixed-species biofilms underwent two washes with PBS to eliminate non-adherent microorganisms, following which they were transferred to a tube containing 1 mL of PBS. Subsequently, the samples were vortexed for 1 minute to collect the biofilm. Culture of the microorganisms was performed using BHI agar plates. These agar plates were then anaerobically incubated at 37°C, varying in duration based on the microorganism: *S. aureus* and *S. mutans* for 2 days, *P. gingivalis* for 5–7 days, and mix-species for 4–7 days, to enumerate CFUs.

Detection of Metabolic Activity of Biofilm

After the incubation of biofilms, samples (n = 6) underwent two washes with PBS to eliminate non-adherent bacteria before being transferred into a new 24-well plate. To assess the metabolic activity of biofilms on test samples, 3-(4, 5-dimethylthiazolyl-2)-2, 5-diphenyltetrazolium bromide (MTT kit, MCE, US) was utilized. Each well received 1 mL of 0.5 mg/mL MTT solution, submerging the test discs. Following a 2-hour incubation at 37°C in a micro-aerobic environment, the MTT solution was replaced with 1 mL of dimethyl sulfoxide (DMSO). After gently shaking the 24-well plate for 20 minutes, 200 μL of DMSO from each well was transferred into a 96-well plate, and the absorbance at 540 nm was measured using a spectrophotometer (Spectra Max iD3, Molecular Devices, US) to evaluate the biofilm's metabolic activity.

Biofilm Imaging

Following incubation, the randomly selected samples with single-species or mixed-species 24-hour biofilms underwent two washes with phosphate buffer solution (PBS) to eliminate non-adherent cells. These samples were then immersed in glutaraldehyde solution (2.5%), dehydrated progressively using ethanol solutions (ranging from 30% to 100%), and

subsequently desiccated. Upon desiccation, gold-sputtering was performed, and adherent microorganisms were visualized using SEM (Sigma 300, Zeiss, Germany).

Statistical Analysis

The experiments were conducted in triplicate and repeated on three separate occasions. Statistical analyses were carried out using SPSS software version 20.0. Outliers were identified using boxplot analysis. The Shapiro–Wilk test was performed to assess normality. For data that followed a normal distribution, one-way ANOVA was employed. In contrast, the Kruskal–Wallis test was used for non-normal data. Levene's test was conducted to check for homogeneity of variances. In cases of heterogeneous variances, Welch's ANOVA was applied. Post hoc analysis for one-way ANOVA involved Tukey's multiple-comparison test for homogeneous data and Dunnett's T3 test for cases with non-homogeneous variances. For the Kruskal–Wallis test, Dunn's Test was utilized for post hoc comparisons. A significance level of $\alpha = 0.05$ was applied to all tests.

Results

Surface Properties

As shown in Figure 1A, the color of both Ti+AO and Ti+ALD samples changed to yellow hue, which is conducive to peri-implant soft tissue color of Ti abutment.[29]

Chemical Analysis

To determine the elemental composition and chemical bonds of the nano-TiO_2 coatings prepared by AO and ALD on Ti abutment surfaces, XPS analysis was performed on the Ti, Ti+AO, and Ti+ALD samples. Figure 1B and Table 1 displayed the full XPS spectrum of the Ti, Ti+AO, Ti+ALD groups, which all had three distinct peaks attributed to Ti, oxygen (O), and carbon (C) elements. Specifically, in the Ti+ALD group, the relative atomic content of C and Ti elements was the highest, accounting for 29.65 at. % and 21.34 at. %, respectively, with trace amounts of Nitrogen (N) detected. In the Ti+AO group, the relative atomic content of O element was the highest, at 51.21 at. %.

The high-resolution Ti2p spectra in Figure 1C showed double peaks at approximately 464.2 eV and 458.5 eV, corresponding to $Ti^{4+}2p_{1/2}$ and $Ti^{4+}2p_{3/2}$, indicating the presence of Ti^{4+}. These peaks were consistent with the reference spectra for TiO_2, confirming that the coatings consisted of TiO_2.[30] Additionally, a broad shoulder peak at 453.8 eV in the Ti group represented the elementary substance Ti, which was not detected in the Ti+AO and Ti+ALD groups, indicating that Ti was successfully oxidized during the AO and ALD processes. Furthermore, the highest relative atomic content of Ti^{4+} (3.04 at.%) was observed in the Ti+ALD group, indicating the highest level of TiO_2. (Table 2) This finding also corresponded to the notably heightened atomic concentration of Ti element (21.34 at.%) in the Ti+ALD group.

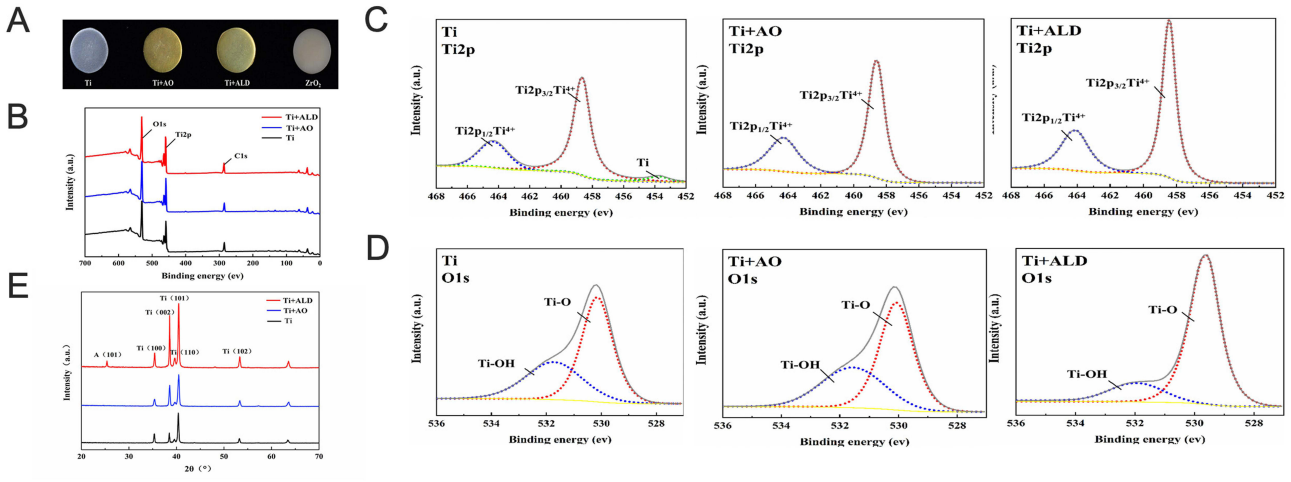

Figure 1 Photographs, Chemical and crystalline forms analysis on surfaces of samples. (**A**) Photographs of samples; (**B**) XPS full spectrum; (**C**) High-resolution scan around Ti element; (**D**) High-resolution scan around O element; (**E**) XRD patterns.

Table 1 Atomic Concentration Percentages of Each Element (at. %)

Group	C	O	Ti	Al	Si	P	N
Ti	28.06	48.78	18.42	2.52	2.22	—	—
Ti+AO	25.02	51.21	17.97	—	2.39	2.09	1.33
Ti+ALD	29.65	47.87	21.34	—	—	—	1.16

Note: "—" signifies the absence of detection.

Table 2 Atomic Concentration Percentages of Chemical Bonds of Main Element (at. %)

Element	Chemical bond	Ti	Ti+AO	Ti+ALD
O1s	Ti-O	4.38	4.55	5.75
	Ti-OH	2.76	3.02	1.56
Ti2p	Ti^{4+}	2.66	2.59	3.04
	Ti	0.20	—	—

Note: "—" signifies the absence of detection.

The high-resolution O1s spectra in Figure 1D showed two peaks at approximately 529.9 eV and 531.7 eV, corresponding to Ti-O and Ti-OH bonds, respectively. Specifically, ALD-TiO_2 exhibited the highest relative atomic content of Ti-O at 5.75 at.%, while Ti-OH showed the lowest presence (1.56 at.%) in this group. (Table 2)

Crystalline Forms Analysis

To determine the crystalline structure of nano-TiO2 coatings prepared by AO and ALD on Ti abutment surfaces, XRD analysis was performed on the Ti, Ti+AO, and Ti+ALD samples, as shown in Figure 1E. The diffraction peaks for the α-phase (100), (002), (101), and (102) planes and the β-phase (110) were observed in all groups. Notably, the Ti+ALD group showed a strong A (101) diffraction peak at 2θ=25.4°, presenting the formation of anatase TiO_2 phase compared to the other groups.

Surface Topography and Roughness Analysis

The surface topography and roughness of Ti, Ti+AO, Ti+ALD, and ZrO_2 groups were examined using SEM and AFM, illustrated in Figure 2A and B. SEM analysis revealed distinctive features: The Ti group displayed non-uniform surface

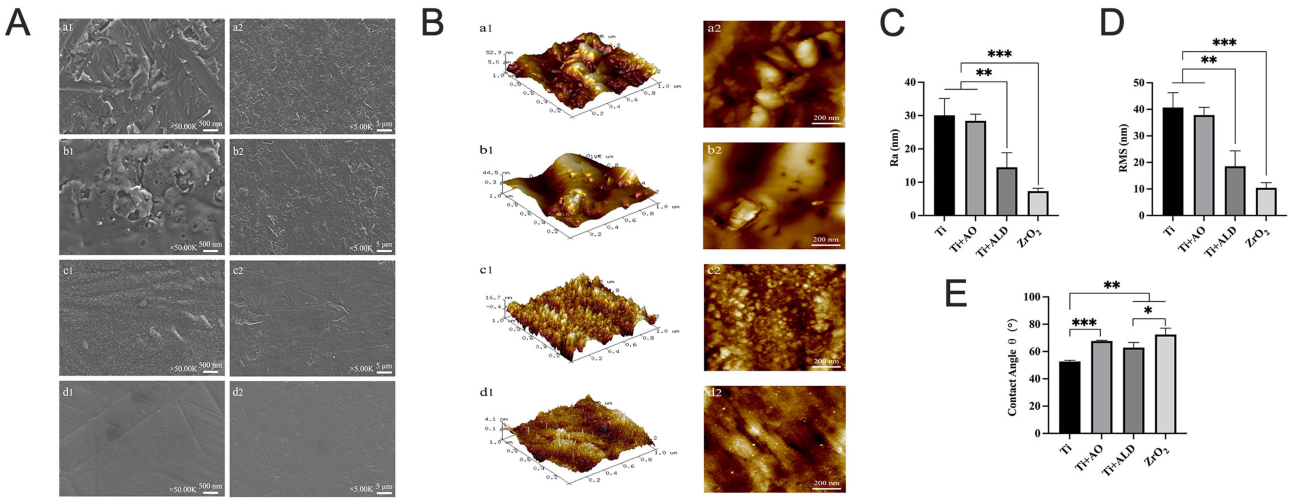

Figure 2 Surface topography, roughness, and hydrophilicity analysis on surfaces of samples. (**A**) SEM; (**B**) AFM morphology. (a) Ti group; (b) Ti+AO group; (c) Ti+ALD group; (d) ZrO_2 group. (**C**) Roughness (Ra); (**D**) Roughness (RMS); (**E**) Water contact angles. *p < 0.05, **p < 0.01, ***p < 0.001.

structures with noticeable tripping and flake formations. Conversely, the Ti+AO group exhibited a smoother surface with reduced and shallower scratches alongside various nano-sized pores on the oxide film. The ALD-TiO_2 coatings appeared denser than the AO-TiO_2 and non-coated surfaces, uniformly covering the substrate with TiO_2 nanoparticles, resulting in a visibly smoother surface. Similarly, the ZrO_2 group displayed a uniformly smooth substrate surface with shallow groove-like scratches, notably smoother than the other groups. AFM images mirrored these trends. The Ti sample displayed ridge-uplift and valley depression, whereas the AO-TiO_2 coated surfaces showed subtle variations with pore-like structures. In contrast, the ALD-TiO_2 coated samples presented the sharp and spikelike nanostructures. The ZrO_2 surface exhibited the smoothest surface (SEM image), featuring densely distributed point-like particles with scattered needle-like protrusions (AFM image).

Additionally, Figure 2C and D presented the roughness values. Compared to the Ti group, the surface roughness (Ra) of the Ti+AO, Ti+ALD, and ZrO2 groups decreased from (30.07 ± 5.06) nm to (28.40 ± 2.01) nm, (14.47 ± 4.39) nm, and (7.33 ± 0.87) nm, respectively. Both Ti and Ti+AO groups were significantly different with Ti+ALD ($p < 0.01$) and ZrO_2 ($p < 0.001$) groups, respectively. However, the differences between the Ti group and the Ti+AO group, as well as between the Ti+ALD group and the ZrO_2 group, were not statistically significant ($p > 0.05$). The value of RMS mirrored these trends.

Hydrophilicity

The water contact angles (WCA) of the ZrO_2 (72.45 ± 4.64)°, Ti+ALD (62.91 ± 3.71)°, and Ti+AO (67.75 ± 0.45)° were found to be higher than that of the Ti group (52.70 ± 0.86)° (Figure 2E), all the difference were significant ($p < 0.01$), indicating that the presence of loaded nano-TiO_2 reduced the hydrophilicity of the Ti substrates, but they are still hydrophilicity materials (WCA < 90°).[31] Furthermore, there were statistical differences between Ti+ALD and ZrO_2 groups ($p < 0.05$).

Antibacterial Capability of Single-Species

Colony-forming Unit (CFU) Counts

In Figure 3A, significant differences in CFU results were observed between the ZrO_2 and Ti+ALD groups compared to the Ti+AO and Ti groups after co-culturing with *S. mutans* ($p < 0.01$), *S. aureus* ($p < 0.001$), and *P. gingivalis* ($p < 0.01$), respectively. The comparable bacterial adhesion ($p > 0.05$) was observed among ZrO_2 and Ti+ALD groups, as well as Ti +AO and Ti groups. Then, the evaluation of the antibacterial effect was determined by comparing the bacteria adhesion of bacteria to the Ti+ALD and ZrO_2 groups with that of Ti group. The result showed the lowest observed antimicrobial effect was about 50% (*S. aureus* and *P. gingivalis*), while the highest one was about 80% (*S. mutans*).

Detection of Metabolic Activity of Biofilm

Similar with the result of CFUs, the significant differences in MTT results (Figure 3B) were observed between the ZrO_2 and Ti+ALD groups compared to the Ti+AO and Ti groups after co-culturing with *S. mutans* ($p < 0.01$), *S. aureus* ($p < 0.05$), and *P. gingivalis* ($p < 0.05$), respectively. The comparable bacterial adhesion ($p > 0.05$) was observed among ZrO_2 and Ti+ALD groups, as well as Ti+AO and Ti groups.

Biofilm Imaging

Generally, the SEM images at low magnification (× 5.00K) (Figure 4) exhibited a lower abundance of three bacterial species in Ti+ALD and ZrO_2 groups.

After 24 h co-culturing with *S. mutans* (Figure 4A), the bacteria of Ti group and Ti+AO group were deposited on the material surface, particularly in irregular areas such as scratches and gullies, and formed chain-like patterns. High magnification SEM (× 20.00K) showed that individual bacteria consisted of multiple "capsule" structures in series, with smooth surfaces, full shapes, and intact envelopes.

After 24 h co-culturing with *S. aureus* (Figure 4B), the Ti and Ti+AO groups displayed bacteria clustered on the material surface in a "grape-like" distribution. In contrast, the Ti+ALD and ZrO_2 groups showed scattered spherical bacteria on the specimen surfaces. High magnification SEM (×20.00K) revealed spherical bacteria, full in shape and with complete envelopes in all groups.

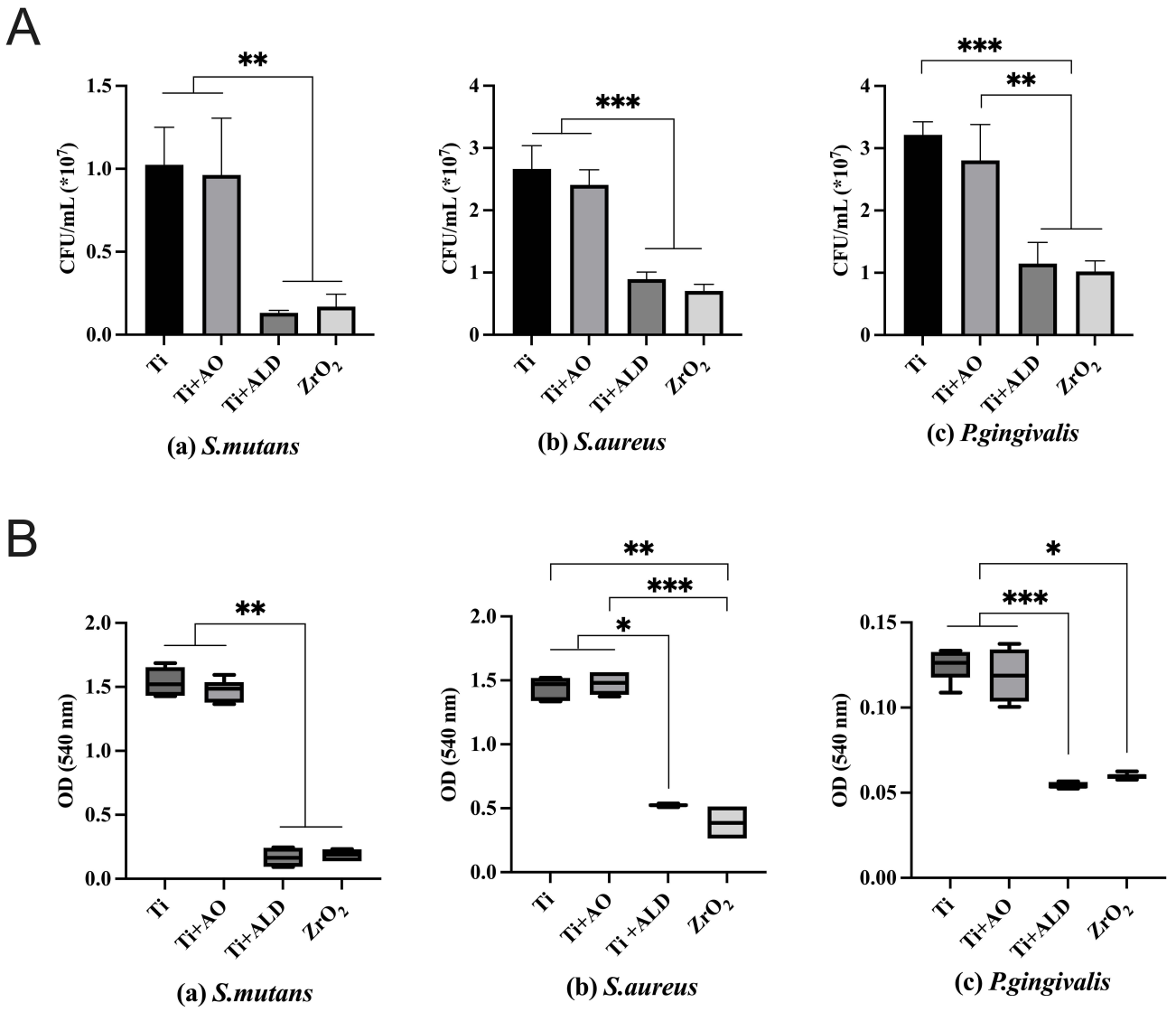

Figure 3 The amount and metabolic activity of bacterial adhesion on surfaces of samples. (**A**) The results of CFUs; (**B**) The results of MTT assay. *$p < 0.05$, **$p < 0.01$, ***$p < 0.001$.

After 24 h co-culturing with *P. gingivalis* (Figure 4C), the Ti and Ti+AO groups exhibited densely dispersed bacteria on the specimen surface. However, the Ti+ALD and ZrO_2 groups showed scattered spherical or rod-shaped bacteria. High magnification SEM (×20.00K) illustrated that individual bacteria were spherical or rod-shaped, with rough surfaces, full shapes, and complete envelopes.

Antibacterial Capability of Mixed-Species

Colony-forming Unit (CFU) Counts

In Figure 5A, significant differences ($p < 0.05$) in CFU results were observed between the ZrO_2 and Ti+ALD groups compared to Ti group after co-culturing with mixed-species consisting of *S. aureus, S. mutans*, and *P. gingivalis*. The comparable bacterial adhesion ($p > 0.05$) was observed between Ti+AO and Ti groups, while significant differences were found among ZrO_2 and Ti+ALD groups ($p < 0.01$), the antibacterial effect was evaluated by comparing bacterial adhesion in the Ti+ALD and ZrO_2 groups with that in the Ti group. The result showed the observed antimicrobial effect was approximately 75% for ALD-TiO_2 and ZrO_2 surfaces.

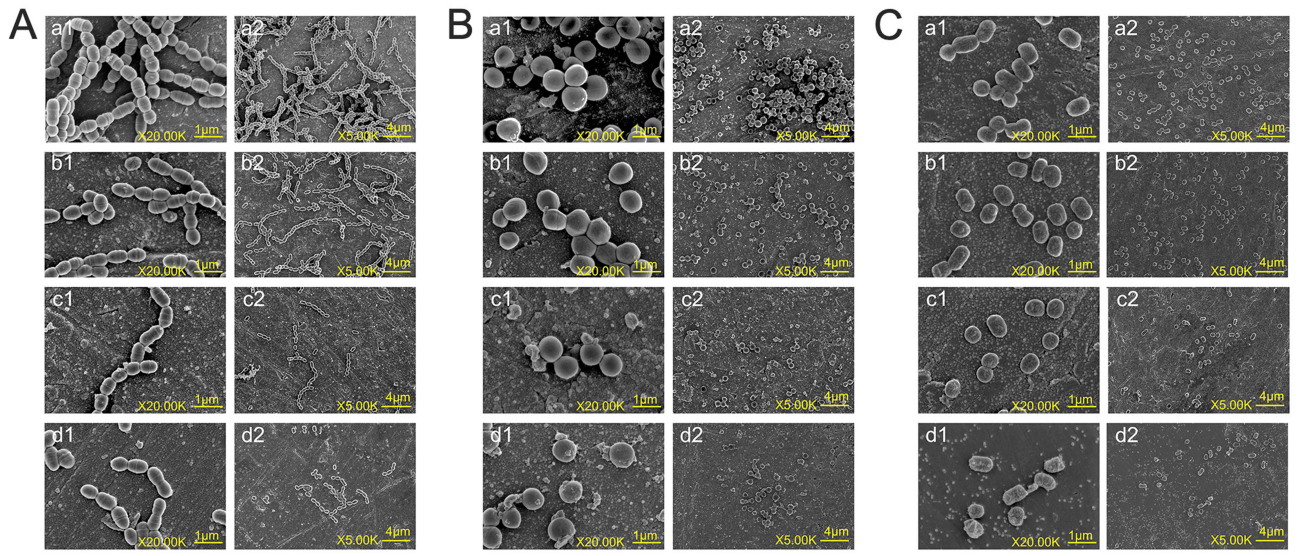

Figure 4 SEM images of biofilms of (**A**) *S. mutans*, (**B**) *S. aureus*, and (**C**) *P. gingivalis* on surfaces of samples. (a) Ti group; (b) Ti+AO group; (c) Ti+ALD group; (d) ZrO_2 group.

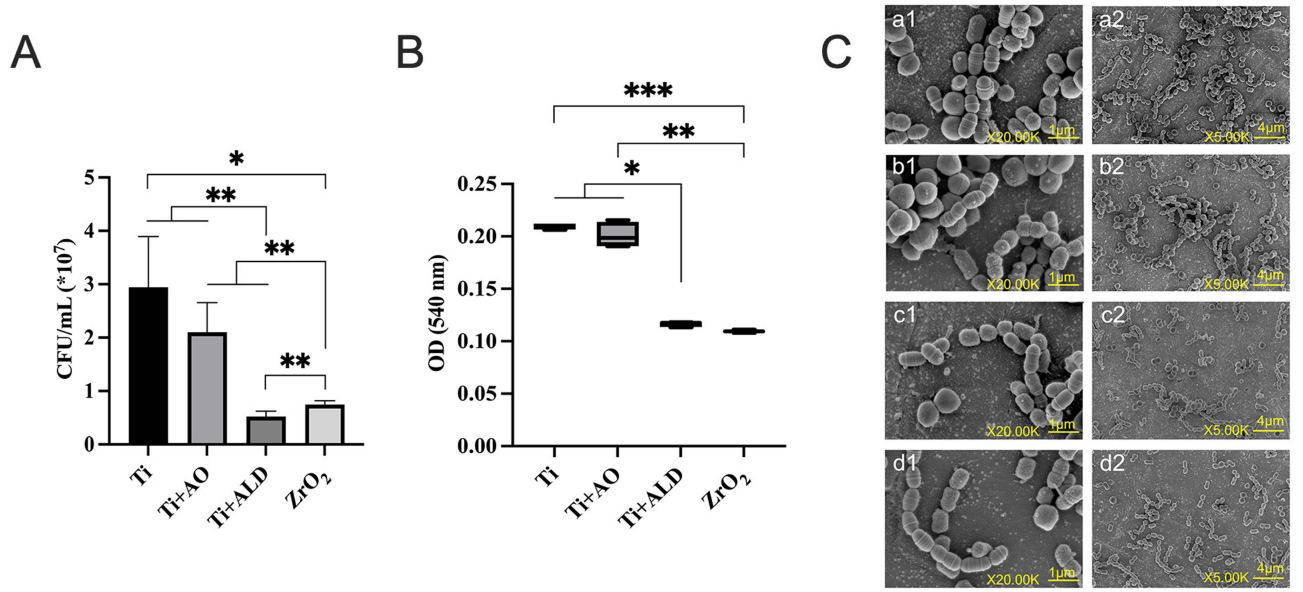

Figure 5 Antibacterial assays for Mixed-Species Biofilm on surfaces of samples. (**A**) The results of CFUs; (**B**) The results of MTT assay; (**C**) SEM images of biofilms (a) Ti group; (b) Ti+AO group; (c) Ti+ALD group; (d)ZrO_2 group. *$p < 0.05$, **$p < 0.01$, ***$p < 0.001$.

Detection of Metabolic Activity of Biofilm

Similar with the result of CFUs, the significant differences ($p < 0.05$) in MTT results (Figure 5B) were observed between the ZrO_2 and Ti+ALD groups compared to the Ti+AO and Ti groups after co-culturing with mixed-species that consist of *S. aureus, S. mutans*, and *P. gingivalis*. The comparable bacterial adhesion ($p > 0.05$) was observed among ZrO_2 and Ti +ALD groups, as well as Ti+AO and Ti groups.

Biofilm Imaging

Low magnification SEM images (×5.00K) (Figure 5C) exhibited that bacteria in the Ti and Ti+AO groups aggregated on the material surface, especially in irregular areas, while the Ti+ALD and ZrO_2 groups had a lower abundance of all three bacterial species.

High magnification SEM (×20.00K) revealed specific characteristics of *S. aureus, S. mutans*, and *P. gingivalis*. *S. aureus* appeared round and larger than the other two bacteria, with a smooth surface, scattered or arranged in "grape-like" clusters. *S. mutans* consisted of several "capsule" structures arranged in chains or singly, with smooth surfaces and full shapes. *P. gingivalis* was bulbous or rod-shaped, with a rough surface, full form, and complete envelope. These three bacteria were interleaved and arranged on the specimen surface.

Discussion

The results indicated a statistically significant difference in surface properties and bacterial adhesion of *S. mutans, S. aureus*, and *P. gingivalis* among the Ti, AO-TiO_2, ALD-TiO_2, and ZrO_2 surfaces. Interestingly, the adhesion of mixed-species bacteria resembled that of single-species bacteria. Consequently, we could accept the first and second null hypotheses while rejecting the third null hypothesis.

Chemical analysis (Figure 1B–D) showed that, in the Ti+ALD group, the relative atomic content of C and Ti elements is the highest, with trace amounts of Nitrogen (N) detected. The presence of C element may originate not only from airborne carbon contamination but also residues of C and N elements from the byproduct generated during the ALD reaction of TDMAT with H_2O, which also explained the source of the detected N element. In the Ti+AO group, the relative atomic content of O element is the highest. This may be attributed to its association with Silicon (Si), Phosphorus (P), and N elements, capable of bonding with O. The Si element, akin to that in the Ti group, might stem from residual Si after polishing with silicon carbide paper on the Ti substrate. It could also originate from the AO process of TiO_2 preparation, explaining the absence of Si element residue in the Ti+ALD group. Prior studies, such as Wang et al,[15] corroborate these findings, noting minor Si and P elements on anodized Ti substrates, suggesting the incorporation of electrolytes into the film-forming process. Additionally, Kern et al[32] indicated the reproducible existence of P in the corresponding oxides during anodization experiments with phosphate-containing electrolytes, where phosphate ions comprised a significant portion of the total film thickness.[33] Phosphate, being a fundamental component of living organisms with good biocompatibility, justifies its selection as an electrolyte in the present study.

The results of Crystalline forms analysis (Figure 1E) indicated that the anatase TiO_2 phase was only found in the Ti +ALD group. This observation is in line with previous studies that reported the formation of the anatase TiO_2 phase through ALD.[17,18] Fenoglio et al[34] found anatase TiO_2 can generate ROS in ambient light conditions (even in darkness) and possesses certain antibacterial properties.[35] Key factors determining the phase structure of nano TiO_2 coatings via ALD technology include precursor types and growth temperatures.[36] Firstly, precursor selection significantly influences the ALD temperature range. Ti alkoxides and amides, commonly used for TiO_2 films, decompose below 300°C and produce non-toxic by-products.[9,37] Accordingly, the present study employed TDMAT as the precursor at temperatures below 300°C. A linear increase in layer thickness with ALD cycles has been observed between 50°C and 300°C.[38] In contrast, Chung et al[39] used the heteroleptic precursor, allowing ALD at temperatures up to 400°C. While halides like $TiCl_4$ also support growth above 400°C, their by-products (eg, HCl) pose corrosion risks.[37] Growth temperature also affects film crystallinity.[9,39,40] Both Reiners et al[40] and Chung et al[39] indicated that higher growth temperature (TDMAT, 250°C and heteroleptic, 236°C) promoted the anatase-phase crystallization, while the lower growth temperature showed amorphous with smooth surfaces. Similarly, Liu et al[9] used TDMAT and H_2O precursors via ALD on Ti implants at temperatures of 120°C, 160°C, and 190°C. Only at 190°C did anatase-phase crystallization occur. In the present study, the ALD reaction temperature was 260°C, exhibiting anatase-phase nano TiO_2 on Ti+ALD samples, consistent with prior researches.[40] However, Ti+AO group lacked anatase diffraction peaks, possibly due to the lower AO voltage (60 V) used herein. Brunello et al used 8 V and 2.2 A for AO modification on Ti alloys, finding similar bacterial adhesion to mechanically processed Ti. In contrast, Giordano et al used 100 V and 120 V for AO, showing anatase diffraction peaks at both voltages, especially intense at higher voltage, indicating electrochemical-induced anatase inhibition against bacterial colonization.[41]

As illustrated in the results of surface topography and roughness analysis (Figure 2), compared to Ti group, Ti+AO group exhibited a smoother surface with reduced and shallower scratches alongside various nano-sized pores on the oxide film. This alteration may be linked to gas emission during AO, consistent with findings from previous studies.[42] The roughness of the Ti+ALD group decreased significantly as a result of particle deposition on the surface, which

partially filled the valley concavities.[43] Furthermore, the surface roughness of the Ti-based substrate decreased after AO and ALD treatments, yet it still did not match the smoothness of the ZrO_2 group, consistent with the observations from the four groups of SEM morphology and AFM surface topography. Nevertheless, the SEM image of ZrO_2 surface exhibited the smoothest surface, while AFM image of that featured densely distributed point-like particles with scattered needle-like protrusions, these were in accordance with other studies.[44–46] The reason for the different surface topography observed in AFM and SEM images is that AFM and SEM differ significantly in terms of imaging mechanisms, resolution, and dimensionality. These two high-resolution surface investigations are complementary techniques that provides a more complete representation of a surface when used together than if each were the only technique available.[47]

Particularly, the AFM and SEM image of Ti+ALD samples exhibited a smooth and spikelike nanostructure. This contrasted with the roughen surfaces observed in other studies,[9,39] likely also due to differences in production parameters of ALD process, such as precursor type, growth temperature, substrate and coating thickness.[37] The influence of precursor type on the growth temperature has been previously discussed. As Chung et al[39] noted, ALD growth temperature significantly affected the film's microstructure, and roughness. Their films grown at 182°C were amorphous with smooth surfaces, while those above 236°C showed the roughening surfaces. At temperatures above 300°C, only very fine grains were apparent. Liu et al[9] also found a remarkable nanorough surfaces at 120°C, 160°C and 190°C. In the present study, the growth temperature of 260°C was applied, which was aligns with the 263°C reported by Chung et al,[39] yet differences in surface morphology persisted. Substrate choice is another factor influencing crystallization behavior.[48,49] The distinct microstructures we observed likely result from the differing substrates used for TiO_2 coating. Additionally, coating thickness plays a key role in determining surface morphology.[18,39,49] Thicker films tend to crystallize,[39] with particle size and crystallization rate increasing with thickness.[18] Beyond a threshold, fewer active O-sites reduce the crystallization rate.[50] Building on our previous findings,[18] the 100 nm ALD-TiO_2 coating not only reduced bacterial adhesion but also exhibited favorable biocompatibility, corrosion resistance, and a warm yellow hue, enhancing the aesthetics of dental abutments. To achieve similar performance and avoid the corrosion risks associated with $TiCl_4$ at high temperatures, we changed the precursor to TDMAT and conducted this ALD process in the present study. It can be found that the similar color, surface properties and antibacterial performance were observed.

The decreased hydrophilicity was found in Ti+AO, Ti+ALD and ZrO_2 groups, these phenomena could stem from the relatively smooth surface of the ALD-TiO_2 and ZrO_2 (Figure 2E), while they might also be attributed to the interaction between surface roughness and hydroxyl density.[42] Further research is needed to explore the extent to which these factors influence water contact angles, as well as the potential involvement of other factors.

Despite the diversity within oral microbial communities, the formation of plaque and the development of biofilms are continuous and dynamic processes. *Streptococcus*, a Gram-positive, facultative anaerobic bacteria with a short doubling time, has been established as an early colonizer on surfaces of teeth and dental implants.[51,52] The late colonizers, represented by slow-growing obligate anaerobes like *P. gingivalis*, gradually integrate into the oral biofilm,[53,54] coinciding with the decrease of early colonization bacteria.[55] Hence, this study selected three bacteria: *S. mutans* and *S. aureus*, both Gram-positive early colonizers, and *P. gingivalis*, a Gram-negative late colonizer and obligate anaerobe. The evaluation of the antibacterial effect was determined by comparing the adhesion of bacteria to the Ti group with that of the other three groups.

This study investigated the antibacterial properties of ZrO_2 and Ti, as well as ALD/AO-TiO_2 on Ti substrates via CFUs and MTT (Figure 3). The ZrO_2 and Ti+ALD groups showed comparable antibacterial properties, while Ti+AO group showed no antibacterial effect. Specifically, the lowest observed antimicrobial effect was about 50% (*S. aureus* and *P. gingivalis*), while the highest one was approximately 80% (*S. mutans*). The higher bactericidal efficacy against Gram-positive *S. mutans* (80%) compared to Gram-negative *P. gingivalis* (50%) was surprising, given the general belief that Gram-positive species are more resistant to mechanical rupture. This discrepancy could be attributed to their different modes of cell division, with *S. aureus* forming clusters and *S. mutans* forming chains. Consequently, *S. mutans* may encounter difficulty dividing laterally across nanostructured surfaces, exposing them to a larger surface area and potentially causing higher levels of membrane stress.[56]

The surface properties of materials play a crucial role in bacterial adhesion and growth, influenced by various factors such as surface roughness, wettability, charge, surface topography, and chemical composition.[57,58] The surface characteristics of the ZrO_2 group exhibited extreme smoothness, uniformity, and absence of pronounced grooves, and show the largest contact angle, indicating the poorest hydrophilicity. This may explain, in part, the reduced bacterial adhesion observed in the ZrO_2 group, aligning with findings from other in vitro[59] and in vivo studies.[4] Another research suggested that ZrO_2 is an amphoteric metal, potentially displaying a positive charge or being neutral.[60] In contrast, the metal Ti surface has an isoelectric point of around 6.0 and carries a negative charge.[61] Bacterial adhesion, facilitated by calcium ions,[11] tends to occur more on negatively charged Ti surfaces, resulting in a localized positive charge. While most bacteria remain negatively charged,[62] which promotes bacterial adhesion on the Ti surface.[63] This elucidated the higher bacterial adhesion observed on Ti surfaces, contributing to the significantly lower bacterial adhesion in the ZrO_2 group within this study. However, bacterial adhesion is a complex process, demanding further investigation into the relative impact of these factors and potential synergistic effects.

On another note, Ti-based substrate materials treated with AO and ALD exhibited an increase in water contact angle, indicating decreased hydrophilicity. Intriguingly, only the Ti+ALD group demonstrated antibacterial properties comparable to the ZrO_2 group. There are several explanations for this phenomenon. Firstly, ALD-TiO_2 effectively concealing deep and extensive scratches and fissures on Ti substrate surfaces. Moreover, the smoother and more hydrophobic surfaces potentially reduced bacteria adherence,[64,65] subsequently inhibiting bacterial capacity to withstand shear forces and proliferate on material surfaces.[8] Secondly, ALD, as a nano-coating technique, leads to densely clustered nanoparticles on TiO_2 coatings. Prior research has highlighted that this augmentation in surface nanostructures diminishes bacterial adhesion by reducing bacterial anchoring points and enhancing fibronectin adsorption.[9,66–68] Hayles et al[56] also demonstrated that spiked titanium nanostructures could eliminate anaerobic dental pathogens in both single-species and dual-species. Similarly, Lorenzetti et al[69] indicated that in TiO_2-coated samples, the nanocrystals reduced the spacing between microasperities, introducing nanoroughness. This decreased the contact area between bacteria and the surface, resulting in up to 50% less bacterial adhesion compared to untreated titanium. Thirdly, ALD technology facilitates the concurrent production of anatase TiO_2 with precise temperature regulation, thereby resulting in heightened antibacterial efficacy in comparison to the amorphous layers of TiO_2 coatings formed on the Ti and Ti+AO group's surfaces.[8,70] Dorkhan et al[16] also confirm that early colonizer adherence diminishes notably on surfaces abundant in anatase (ALD-TiO_2). Another reason for the relatively poorer antibacterial performance of the Ti+AO group might be its similarity in roughness to the Ti group. Additionally, SEM images (Figure 4) indicated a more porous surface morphology of AO-TiO_2, which further facilitates bacterial adhesion.[64,65]

The SEM images (Figure 4) exhibited a lower abundance of three bacteria in Ti+ALD and ZrO_2 groups. Moreover, all the bacteria formed thick membrane with geometric three-dimensional complexity, suggesting the absence of obvious bactericide mechanism of ALD-TiO_2. This may be attributed to the limitations of nano-TiO_2 as a bactericide, which is in nanoparticle form and relies on photofunctionalization.[8]

Apart from material surface physicochemical properties, competitive interactions among bacteria within mixed-species environments also might impact the extent of bacterial adhesion. This behavior might stem from bacterial competition for nutrients and/or inhibition by other species, with varying inhibitory activities among different bacterial species. For instance, Li et al[71] observed that *S. mutans* biofilm cells predominated in mixed cultures due to shorter generation times, thus having an advantage in competition with other bacterial species. Tu et al[72] also confirmed the supernatants from *S. mutans* markedly suppressed the growth and biofilm formation of *P. gingivalis*. Moreover, metabolic interactions and signaling molecules between bacteria contribute to the maturity of biofilms.[73] Multi-species biofilms generate extracellular polymeric substances (EPS) that consist of polysaccharides, proteins, and extracellular DNA, aggregating them favorably in three-dimensional spatial arrangements.[74]

To better simulate the oral environment, considering bacterial proliferation time and nutrient competition, a mixed in vitro bacterial model comprising three species was constructed in the present study. Initial concentrations in the mixed model were set as 1×10^3 CFU/mL for *S. mutans* and *S. aureus*, and 1×10^8 CFU/mL for *P. gingivalis*, enabling the coexistence and reproduction of the three strains, which also aligns with the decline in the early colonization bacteria proportion when *P. gingivalis* participates in biofilm formation.[55] Interestingly, SEM observations and MTT assay results

(Figure 5) indicated that bacterial adhesion on the surfaces of the four groups correlated with the trend observed for single-species adhesion. The only variation noted was in the CFU results for the mixed-species cultures, where the Ti +ALD group had a significantly lower CFU count than the ZrO_2 group ($p<0.01$). However, the MTT assay showed similar metabolic activity between the two groups. This discrepancy arises from differences in the assay principles. The CFU assay measures the number of viable cells capable of colony formation, while the MTT assay assesses metabolic activity by measuring the reduction of MTT to formazan crystals, indicating cell viability.[75] Therefore, a sample with high metabolic activity (reflected in MTT results) may not have a corresponding high CFU count, especially if some cells are alive but not replicating. Additionally, interactions in mixed-species cultures can affect bacterial growth and metabolism. For example, some oral bacterial strains, such as *S.mutans*, can inhibit growth of *P. gingivalis* through various mechanisms,[72,76] which could lead to a lower CFU count but sustained metabolic activity. Although the CFU results showed that the Ti+ALD group had significantly lower bacterial counts than the ZrO_2 group, the values for them were notably low compared to Ti+AO and Ti groups. Based on the mixed-species MTT results and the CFU and MTT results for single species, the antibacterial efficacy of the ALD-TiO_2 coating and the ZrO_2 surface remains comparable. This suggested that, in a more complex environment containing multiple bacteria, the Ti+ALD and ZrO_2 groups, influenced by the physicochemical properties of the material surface, still exhibit the least bacterial adhesion compared to the Ti and Ti+AO groups, making them ideal choices for dental abutment materials.

However, although this study's inclusion of three peri-implantitis-related bacterial species adds complexity compared to other single-species in vitro studies, limitations in the complexity of the oral microbial environment mean it is still distant from the human oral microbiome. Further investigations will aim to optimize bacterial growth conditions, simulate the surrounding environment more accurately, including microbial diversity and relationships, providing potential laboratory-based evidence for the selection of clinical abutment materials. Furthermore, the perimucosal integration surrounding the abutment serves as the initial defense against pathogenic infiltration leading to peri-implantitis. Consequently, the surface characteristics of the abutment profoundly influence this soft tissue response. Thus, the effects of nano-TiO_2 coatings prepared by ALD and AO technologies on soft tissue integration also need further investigation.

Conclusion

With the limitation of this study, the following conclusions were drawn.

1. Nano-TiO_2 coatings prepared by ALD rendered the surface of dental Ti abutment dense, flat, smooth, and less hydrophilia, featuring an anatase phase. This modification significantly reduced the adhesion of *S. aureus, S. mutans*, and *P. gingivalis*, by at least 50%, comparable to the effect observed on ZrO_2 surfaces.
2. Nano-TiO_2 coatings prepared by AO made the surface of dental Ti abutment less hydrophilia, characterized by various nano-sized pores within the oxide film. However, this alteration did not impact the adhesion of *S. aureus, S. mutans*, and *P. gingivalis*.
3. The adhesion behavior of mixed-species bacteria (consisting of the aforementioned three species) closely mirrored that of single-species bacteria. It confirmed that, akin to ZrO_2 abutments, nano-TiO_2 coatings prepared by ALD on Ti abutments exhibited strong potential for application in preventing peri-implantitis. In contrast, the antibacterial efficacy of AO-TiO_2 abutments was not obvious, resembling that of Ti abutments.

Acknowledgments

Thanks to Prof. Zhijian Hu, Public Health School of Fujian Medical University, for his guidance on statistic and Prof. Hao Yu, School and Hospital of Stomatology of Fujian Medical University, for English editing and valuable comments.

Funding

This work was supported by Fujian Provincial Financial Special Fund (22SCZZX008); Fujian Provincial University-Industry Cooperation Project (2022Y4006); Fujian Province Natural Science Foundation of China (2022J01268 and 2023J01708); and Fujian Provincial Health Technology Project (2022QNB003).

Disclosure

The authors report no conflicts of interest in this work.

References

1. Guo C, Lu R, Wang X, Chen S. Graphene oxide-modified polyetheretherketone with excellent antibacterial properties and biocompatibility for implant abutment. *Macromol Res*. 2021;29(5):351–359. doi:10.1007/s13233-021-9042-3
2. Atsuta I, Ayukawa Y, Kondo R, et al. Soft tissue sealing around dental implants based on histological interpretation. *J Prosthodont Res*. 2016;60(1):3–11. doi:10.1016/j.jpor.2015.07.001
3. Huang YS, Huang HH. Effects of clinical dental implant abutment materials and their surface characteristics on initial bacterial adhesion. *Rare Met*. 2019;38(6):512–519. doi:10.1007/s12598-019-01219-0
4. Sanz-Martin I, Sanz-Sanchez I, Carrillo de Albornoz A, Figuero E, Sanz M. Effects of modified abutment characteristics on peri-implant soft tissue health: a systematic review and meta-analysis. *Clin Oral Implants Res*. 2018;29(1):118–129. doi:10.1111/clr.13097
5. Nakamura K, Kanno T, Milleding P, Ortengren U. Zirconia as a dental implant abutment material: a systematic review. *Int J Prosthodont*. 2010;23(4):299–309.
6. Wiedmer D, Cui C, Weber F, Petersen FC, Tiainen H. Antibacterial surface coating for bone scaffolds based on the dark catalytic effect of titanium dioxide. *ACS Appl Mater Interfaces*. 2018;10(42):35784–35793. doi:10.1021/acsami.8b12623
7. Rawat N, Bencina M, Gongadze E, Junkar I, Iglic A. Fabrication of antibacterial TiO_2 nanostructured surfaces using the hydrothermal method. *ACS Omega*. 2022;7(50):47070–47077. doi:10.1021/acsomega.2c06175
8. Pantaroto HN, Ricomini-Filho AP, Bertolini MM, et al. Antibacterial photocatalytic activity of different crystalline TiO_2 phases in oral multispecies biofilm. *Dent Mater*. 2018;34(7):e182–e195. doi:10.1016/j.dental.2018.03.011
9. Liu L, Bhatia R, Webster TJ. Atomic layer deposition of nano-TiO_2 thin films with enhanced biocompatibility and antimicrobial activity for orthopedic implants. *Int J Nanomed*. 2017;12:8711–8723. doi:10.2147/IJN.S148065
10. Tuikampee S, Chaijareenont P, Rungsiyakull P, Yavirach A. Titanium surface modification techniques to enhance osteoblasts and bone formation for dental implants: a narrative review on current advances. *Metals*. 2024;14(5):515. doi:10.3390/met14050515
11. Badihi Hauslich L, Sela MN, Steinberg D, Rosen G, Kohavi D. The adhesion of oral bacteria to modified titanium surfaces: role of plasma proteins and electrostatic forces. *Clin Oral Implants Res*. 2013;24(A100):49–56. doi:10.1111/j.1600-0501.2011.02364.x
12. Ragucci GM, Giralt-Hernando M, Mendez-Manjon I, Canto-Naves O, Hernandez-Alfaro F. Factors affecting implant failure and marginal bone loss of implants placed by post-graduate students: a 1-year prospective cohort study. *Materials*. 2020;13(20):4511. doi:10.3390/ma13204511
13. Lin WS, Harris BT, Zandinejad A, Morton D. Use of digital data acquisition and CAD/CAM technology for the fabrication of a fixed complete dental prosthesis on dental implants. *J Prosthet Dent*. 2014;111(1):1–5. doi:10.1016/j.prosdent.2013.04.010
14. Diamanti MV, Del Curto B, Pedeferri M. Anodic oxidation of titanium: from technical aspects to biomedical applications. *J Appl Biomater Biomech*. 2011;9(1):55–69. doi:10.5301/JABB.2011.7429
15. Wang T, Wang L, Lu Q, Fan Z. Changes in the esthetic, physical, and biological properties of a titanium alloy abutment treated by anodic oxidation. *J Prosthet Dent*. 2019;121(1):156–165. doi:10.1016/j.prosdent.2018.03.024
16. Dorkhan M, Hall J, Uvdal P, Sandell A, Svensäter G, Davies JR. Crystalline anatase-rich titanium can reduce adherence of oral streptococci. *Biofouling*. 2014;30(6):751–759. doi:10.1080/08927014.2014.922962
17. Hall J, Neilands J, Davies JR, Ekestubbe A, Friberg B. A randomized, controlled, clinical study on a new titanium oxide abutment surface for improved healing and soft tissue health. *Clin Implant Dent Relat Res*. 2019;21 Suppl 1(S1):55–68. doi:10.1111/cid.12749
18. Gao L, Wu K, Wei X, et al. Evaluation of antibacterial activity and biocompatibility of nano-titanium dioxide coatings prepared by atomic layer deposition for dental titanium abutments. *Surf Interfaces*. 2024;48:104280. doi:10.1016/j.surfin.2024.104280
19. Oviroh PO, Akbarzadeh R, Pan D, Coetzee RAM, Jen TC. New development of atomic layer deposition: processes, methods and applications. *Sci Technol Adv Mater*. 2019;20(1):465–496. doi:10.1080/14686996.2019.1599694
20. Jo Y, Kim YT, Cho H, Ji M-K, Heo J, Lim H-P. Atomic layer deposition of ZrO_2 on titanium inhibits bacterial adhesion and enhances osteoblast viability. *Int J Nanomed*. 2021;16:1509–1523. doi:10.2147/IJN.S298449
21. Darwish G, Huang S, Knoernschild K, et al. Improving polymethyl methacrylate resin using a novel titanium dioxide coating. *J Prosthodont*. 2019;28(9):1011–1017. doi:10.1111/jopr.13032
22. do NC, Sucena PM, Carriço FFHN, Vinícius P, Ferreira D, Faria RR. Bacterial adhesion on the titanium and zirconia abutment surfaces. *Clin Oral Implants Res*. 2014;25(3):337–343. doi:10.1111/clr.12093
23. Deepak D, Trishla S. Biofilm development in gram-positive and gram-negative bacteria. In: Theerthankar D, editor. *Focus on Bacterial Biofilms*. IntechOpen; 2022:Ch.6.
24. Ruhal R, Kataria R. Biofilm patterns in gram-positive and gram-negative bacteria. *Microbiol Res*. 2021;251:126829. doi:10.1016/j.micres.2021.126829
25. Vengadesan K, Narayana SV. Structural biology of Gram-positive bacterial adhesins. *Protein Sci*. 2011;20(5):759–772. doi:10.1002/pro.613
26. Kumaravel V, Nair KM, Mathew S, et al. Antimicrobial TiO_2 nanocomposite coatings for surfaces, dental and orthopaedic implants. *Chem Eng J*. 2021;416:129071. doi:10.1016/j.cej.2021.129071
27. Mark Welch JL, Rossetti BJ, Rieken CW, Dewhirst FE, Borisy GG. Biogeography of a human oral microbiome at the micron scale. *Proc Natl Acad Sci U S A*. 2016;113(6):791–800. doi:10.1073/pnas.1522149113
28. Mouratidou A, Karbach J, d'Hoedt B, Al-Nawas B. Antibiotic susceptibility of cocultures in polymicrobial infections such as peri-implantitis or periodontitis: an in vitro model. *J Periodontol*. 2011;82(9):1360–1366. doi:10.1902/jop.2011.100657
29. Wadhwani CP, O'Brien R, Kattadiyil MT, Chung KH. Laboratory technique for coloring titanium abutments to improve esthetics. *J Prosthet Dent*. 2016;115(4):409–411. doi:10.1016/j.prosdent.2015.09.024
30. Sul YT, Johansson CB, Petronis S, et al. Characteristics of the surface oxides on turned and electrochemically oxidized pure titanium implants up to dielectric breakdown: the oxide thickness, micropore configurations, surface roughness, crystal structure and chemical composition. *Biomaterials*. 2002;23(2):491–501. doi:10.1016/S0142-9612(01)00131-4

31. Vuckovac M, Latikka M, Liu K, Huhtamäki T, Ras RHA. Uncertainties in contact angle goniometry. *Soft Matter*. 2019;15(35):7089–7096. doi:10.1039/C9SM01221D
32. Kern P, Schwaller P, Michler J. Electrolytic deposition of titania films as interference coatings on biomedical implants: microstructure, chemistry and nano-mechanical properties. *Thin Solid Films*. 2005;494(1):279–286. doi:10.1016/j.tsf.2005.09.068
33. Habazaki H, Shimizu K, Nagata S, Skeldon P, Thompson GE, Wood GC. Ionic transport in amorphous anodic titania stabilised by incorporation of silicon species. *Corros Sci*. 2002;44(5):1047–1055. doi:10.1016/S0010-938X(01)00111-1
34. Fenoglio I, Greco G, Livraghi S, Fubini B. Non-UV-induced radical reactions at the surface of TiO_2 nanoparticles that may trigger toxic responses. *Chemistry*. 2009;15(18):4614–4621. doi:10.1002/chem.200802542
35. Arturs M, Pavels O, Jevgenis K, et al. Anatase or rutile TiO_2 nanolayer formation on Ti substrates by laser radiation: mechanical, photocatalytic and antibacterial properties. *Opt Laser Technol*. 2021;138:106898. doi:10.1016/j.optlastec.2020.106898
36. Biyikli N, Haider A. Atomic layer deposition: an enabling technology for the growth of functional nanoscale semiconductors. *Semicond Sci Technol*. 2017;32(9):093002. doi:10.1088/1361-6641/aa7ade
37. Niemelä J-P, Marin G, Karppinen M. Titanium dioxide thin films by atomic layer deposition: a review. *Semicond Sci Technol*. 2017;32(9):093005. doi:10.1088/1361-6641/aa78ce
38. Aarik J, Aidla A, Mändar H, Uustare T. Atomic layer deposition of titanium dioxide from $TiCl_4$ and H_2O: investigation of growth mechanism. *Appl Surf Sci*. 2001;172(1):148–158. doi:10.1016/S0169-4332(00)00842-4
39. Chung HK, Won SO, Park Y, Kim J-S, Park TJ, Kim SK. Atomic-layer deposition of TiO_2 thin films with a thermally stable $(CpMe_5)Ti(OMe)_3$ precursor. *Appl Surf Sci*. 2021;550:149381. doi:10.1016/j.apsusc.2021.149381
40. Reiners M, Xu K, Aslam N, Devi A, Waser R, Hoffmann-Eifert S. Growth and crystallization of TiO_2 thin films by atomic layer deposition using a novel amido guanidinate titanium source and tetrakis-dimethylamido-titanium. *Chem Mater*. 2013;25(15):2934–2943. doi:10.1021/cm303703r
41. Giordano C, Saino E, Rimondini L, et al. Electrochemically induced anatase inhibits bacterial colonization on titanium grade 2 and Ti6Al4V alloy for dental and orthopedic devices. *Colloids Surf B Biointerfaces*. 2011;88(2):648–655. doi:10.1016/j.colsurfb.2011.07.054
42. Azimi M, Asselin E. Improving surface functionality, hydrophilicity, and interfacial adhesion properties of high-density polyethylene with activated peroxides. *ACS Appl Mater Interfaces*. 2022;14(2):3601–3609. doi:10.1021/acsami.1c23703
43. Nikkola J, Sievänen J, Raulio M, Wei J, Vuorinen J, Tang CY. Surface modification of thin film composite polyamide membrane using atomic layer deposition method. *J Membr Sci*. 2014;450:174–180. doi:10.1016/j.memsci.2013.09.005
44. de Carvalho IHG, da Silva NR, Vila-Nova TEL, et al. Effect of finishing/polishing techniques and aging on topography, C. albicans adherence, and flexural strength of ultra-translucent zirconia: an in situ study. *Clin Oral Investig*. 2022;26(1):889–900. doi:10.1007/s00784-021-04068-3
45. Park C, Vang MS, Park SW, Lim HP. Effect of various polishing systems on the surface roughness and phase transformation of zirconia and the durability of the polishing systems. *J Prosthet Dent*. 2017;117(3):430–437. doi:10.1016/j.prosdent.2016.10.005
46. Incesu E, Yanikoglu N. Evaluation of the effect of different polishing systems on the surface roughness of dental ceramics. *J Prosthet Dent*. 2020;124(1):100–109. doi:10.1016/j.prosdent.2019.07.003
47. Russell P, Batchelor D, Thornton J. SEM and AFM: complementary techniques for high resolution surface investigations. *Veeco Instrument*. 2001;1:2004.
48. Pessoa RS, Dos Santos VP, Cardoso SB, et al. TiO_2 coatings via atomic layer deposition on polyurethane and polydimethylsiloxane substrates: properties and effects on C. albicans growth and inactivation process. *Appl Surf Sci*. 2017;422:73–84. doi:10.1016/j.apsusc.2017.05.254
49. Puurunen RL, Sajavaara T, Santala E, et al. Controlling the crystallinity and roughness of atomic layer deposited titanium dioxide films. *J Nanosci Nanotechnol*. 2011;11(9):8101–8107. doi:10.1166/jnn.2011.5060
50. Chiappim W, Testoni GE, De lima JSB, et al. Effect of process temperature and reaction cycle number on atomic layer deposition of TiO_2 thin films using TiCl4 and H2O precursors: correlation between material properties and process environment. *Braz J Phys* 2015;46(1):56–69.
51. Furst MM, Salvi GE, Lang NP, Persson GR. Bacterial colonization immediately after installation on oral titanium implants. *Clin Oral Implants Res*. 2007;18(4):501–508. doi:10.1111/j.1600-0501.2007.01381.x
52. Mombelli A, Schmid B, Rutar A, Lang NP. Local antibiotic therapy guided by microbiological diagnosis. *J Clin Periodontol*. 2002;29(8):743–749. doi:10.1034/j.1600-051X.2002.290811.x
53. Siddiqui DA, Fidai AB, Natarajan SG, Rodrigues DC. Succession of oral bacterial colonizers on dental implant materials: an in vitro biofilm model. *Dent Mater*. 2022;38(2):384–396. doi:10.1016/j.dental.2021.12.021
54. Wake N, Asahi Y, Noiri Y, et al. Temporal dynamics of bacterial microbiota in the human oral cavity determined using an in situ model of dental biofilms. *NPJ Biofilms Microbiomes*. 2016;2(1):16018. doi:10.1038/npjbiofilms.2016.18
55. Sánchez MC, Llama-Palacios A, Blanc V, León R, Herrera D, Sanz M. Structure, viability and bacterial kinetics of an in vitro biofilm model using six bacteria from the subgingival microbiota. *J Periodontal Res*. 2011;46(2):252–260. doi:10.1111/j.1600-0765.2010.01341.x
56. Hayles A, Hasan J, Bright R, et al. Spiked titanium nanostructures that inhibit anaerobic dental pathogens. *ACS Appl Nano Mater*. 2022;5(9):12051–12062. doi:10.1021/acsanm.1c04073
57. Esfahanizadeh N, Mirmalek SP, Bahador A, Daneshparvar H, Akhoundi N, Pourhajibagher M. Formation of biofilm on various implant abutment materials. *Gen Dent*. 2018;66(5):39–44.
58. de Avila ED, Avila-Campos MJ, Vergani CE, Spolidorio DMP, Mollo FD. Structural and quantitative analysis of a mature anaerobic biofilm on different implant abutment surfaces. *Article J Prosthet Dent*. 2016;115(4):428–436. doi:10.1016/j.prosdent.2015.09.016
59. Al-Radha ASD, Dymock D, Younes C, O'Sullivan D. Surface properties of titanium and zirconia dental implant materials and their effect on bacterial adhesion. *J Dent*. 2012;40(2):146–153. doi:10.1016/j.jdent.2011.12.006
60. Wei WCJ, Wang S, Ho F. Electrokinetic properties of colloidal zirconia powders in aqueous suspension. *J Am Ceram Soc*. 2010;82(12):3385–3392. doi:10.1111/j.1151-2916.1999.tb02255.x
61. McNamee CE, Tsujii Y, Matsumoto M. Physicochemical characterization of an anatase TiO_2 surface and the adsorption of a nonionic surfactant: an atomic force microscopy study. *Langmuir*. 2005;21(24):11283–11288. doi:10.1021/la0517890
62. Bock RM, Jones EN, Ray DA, Sonny Bal B, Pezzotti G, McEntire BJ. Bacteriostatic behavior of surface modulated silicon nitride in comparison to polyetheretherketone and titanium. *J Biomed Mater Res A*. 2017;105(5):1521–1534. doi:10.1002/jbm.a.35987
63. Oda Y, Miura T, Mori G, et al. Adhesion of streptococci to titanium and zirconia. *PLoS One*. 2020;15(6):e0234524. doi:10.1371/journal.pone.0234524

64. Chan Y, Wu XH, Chieng BW, Ibrahim NA, Then YY. Superhydrophobic nanocoatings as intervention against biofilm-associated bacterial infections. *Nanomaterials*. 2021;11(4):1046. doi:10.3390/nano11041046
65. Wu S, Zhang B, Liu Y, Suo X, Li H. Influence of surface topography on bacterial adhesion: a review (Review). *Biointerphases*. 2018;13(6):060801. doi:10.1116/1.5054057
66. Anagnostou F, Debet A, Pavon-Djavid G, Goudaby Z, Hélary G, Migonney V. Osteoblast functions on functionalized PMMA-based polymers exhibiting Staphylococcus aureus adhesion inhibition. *Biomaterials*. 2006;27(21):3912–3919. doi:10.1016/j.biomaterials.2006.03.004
67. Khang D, Kim SY, Liu-Snyder P, Palmore GT, Durbin SM, Webster TJ. Enhanced fibronectin adsorption on carbon nanotube/poly(carbonate) urethane: independent role of surface nano-roughness and associated surface energy. *Biomaterials*. 2007;28(32):4756–4768. doi:10.1016/j.biomaterials.2007.07.018
68. Kinnari TJ, Peltonen LI, Kuusela P, Kivilahti J, Könönen M, Jero J. Bacterial adherence to titanium surface coated with human serum albumin. *Otol Neurotol*. 2005;26(3):380–384. doi:10.1097/01.mao.0000169767.85549.87
69. Lorenzetti M, Dogša I, Stošicki T, et al. The influence of surface modification on bacterial adhesion to titanium-based substrates. *ACS Appl Mater Interfaces*. 2015;7(3):1644–1651. doi:10.1021/am507148n
70. Huang L, Jing S, Zhuo O, Meng X, Wang X. Surface hydrophilicity and antifungal properties of TiO_2 films coated on a Co-Cr Substrate. *Biomed Res Int*. 2017;2017:2054723. doi:10.1155/2017/2054723
71. Shijia L, Qiuyu C, Jing Z, Ruijie H. Effect of nicotine on the growth of oral bacteria in single or mixed species. *Int J Stomatol*. 2021;48(3):305–311.
72. Tu Y, Ling X, Chen Y, Wang Y, Zhou N, Chen H. Effect of *S. Mutans* and *S. Sanguinis* on growth and adhesion of *P. Gingivalis* and their ability to adhere to different dental materials. *Med Sci Monit*. 2017;23:4539–5445. doi:10.12659/MSM.904114
73. Eick S, Kindblom C, Mizgalska D, et al. Adhesion of porphyromonas gingivalis and tannerella forsythia to dentin and titanium with sandblasted and acid etched surface coated with serum and serum proteins: an in vitro study. *Arch Oral Biol*. 2017;75:81–88. doi:10.1016/j.archoralbio.2016.11.001
74. Wang L, Li C, Weir MD, et al. Novel multifunctional dental bonding agent for Class-V restorations to inhibit periodontal biofilms. *RSC Adv*. 2017;7(46):29004–29014. doi:10.1039/C6RA28711E
75. Xu W, Shi D, Chen K, Palmer J, Popovich DG. An improved MTT colorimetric method for rapid viable bacteria counting. *J Microbiol Methods*. 2023;214:106830. doi:10.1016/j.mimet.2023.106830
76. Tenorio EL, Klein BA, Cheung WS, Hu LT. Identification of interspecies interactions affecting Porphyromonas gingivalis virulence phenotypes. *J Oral Microbiol*. 2011;3(1):8396. doi:10.3402/jom.v3i0.8396